HHS Public Access

Author manuscript

Nat Med. Author manuscript; available in PMC 2013 September 01.

Published in final edited form as:

Nat Med. 2013 March ; 19(3): 313–321. doi:10.1038/nm.3082.

An inhibitor of the protein kinases TBK1/IKKε improves obesity-related metabolic dysfunctions

Shannon M. Reilly[1,*], **Shian-Huey Chiang**[1,*], **Stuart J. Decker**[1], **Louise Chang**[1], **Maeran Uhm**[1,2], **Martha J. Larsen**[1], **John R. Rubin**[1], **Jonathan Mowers**[1,2], **Nicole M. White**[1], **Irit Hochberg**[1], **Michael Downes**[3], **Ruth Yu**[3], **Christopher Liddle**[4], **Ronald M. Evans**[3], **Dayoung Oh**[5], **Pingping Li**[5], **Jerrold M. Olefsky**[5], and **Alan R. Saltiel**[1,2,**]

[1]Life Sciences Institute, University of Michigan, Ann Arbor, MI

[2]Departments of Internal Medicine and Molecular and Integrative Physiology, University of Michigan, Ann Arbor, MI

[3]Salk Institute for Biological Sciences, La Jolla, CA

[4]Storr Liver Unit, Westmead Millennium Institute and University of Sydney, Westmead Hospital, Westmead, New South Wales 2145, Australia

[5]Department of Medicine, University of California, San Diego, San Diego, CA

Abstract

Emerging evidence suggests that inflammation provides a link between obesity and insulin resistance. The noncanonical IκB kinases IKKε and TANK-binding kinase 1 (TBK1) are induced in liver and fat after high fat diet by NF-κB activation, and in turn initiate a program of counter-inflammation that preserves energy storage. Here, we report the discovery of a small molecule inhibitor of these kinases called amlexanox. Treatment of obese mice with amlexanox elevates energy expenditure through increased thermogenesis, producing weight loss, improved insulin sensitivity and decreased steatosis in obese mice. Because of its record of safety in patients, amlexanox may be an interesting candidate for clinical evaluation in the treatment of obesity and related disorders.

**to whom correspondence should be addressed at saltiel@umich.edu.

*These authors contributed equally to this work

Author Contributions.

A.S. and S.R. wrote the manuscript. S.R. created figures. S.R. produced data in Figs. 1e, 3e,i, 4f–i, 5c,f–h, and 6c–j, and Supplementary Figs. 1, 2c–h, 5b,e,g,h, and 6a,b. S.C. produced data in Figs. 3a–d,f–h,j, 4a–e, 5a,c,d,e, 6a,b, and Supplementary Figs. 2a,b, 3, and 5a,d,f. S.D. and M.L. performed the screen identifying amlexanox as an IKKε inhibitor. L.C. and S.D. produced data in Fig. 1b, and Fig. 2b,c,f.

M.U. produced data in Figs. 1a and 2e, and Supplementary Figs. 5c, and 6c–e.

J.R. produced images in Fig. 1d. J.M. produced data in Fig. 1c. N.W. produced data in Supplementary Fig. 4a–d. I.H. produced data in Supplementary Fig. 4e. M.D., R.Y., C.L., and R.E. contributed data not shown, which was instrumental in generating Fig. 5f–h. D.O. produced data in Fig. 1d and samples for Fig. 1e, and P.L. produced data in Fig. 1f under the guidance of J.O.

Introduction

While the molecular events underlying the relationship between obesity and insulin resistance remain uncertain [1–4], numerous studies have implicated an inflammatory link [5–7]. Obesity produces a state of chronic, low-grade inflammation in liver and fat, accompanied by the local secretion of cytokines and chemokines that attenuate insulin action. Knockout or pharmacological inhibition of inflammatory pathways can disrupt the link between genetic or diet-induced obesity and insulin resistance, suggesting that local inflammation is a key step in the generation of insulin resistance in liver and fat [7–11].

The NF-κB transcriptional program is activated in obese fat and liver, and to a lesser extent in muscle, and appears to play an important role in insulin resistance [12–15]. NF-κB activation is triggered by the phosphorylation of the regulatory protein IκB. Four different IκB kinases (IKK) have been identified, IKKα and β, IKKε and TANK-binding kinase 1(TBK1). A role for IKKα and β in NF-κB activation is firmly established, but whether TBK1 and IKKε regulate the pathway remains uncertain [16–18]. However, the genes encoding both of these kinases contain kappaB regulatory sites in their promoter regions, and activation of the NF-κB transcriptional pathway induces their expression [19], suggesting that they may act downstream of this transcriptional pathway.

We recently reported that expression of both *Tbk1* and *Ikbke* mRNA and TBK1 and IKKε protein are increased during high fat diet (HFD) in adipose tissue, while IKKε is increased in liver [15]. Moreover, deletion of the *Ikbke* gene rendered mice partially resistant to the HFD-dependent development of obesity, insulin sensitivity, hepatic steatosis and inflammation, leading us to search for small molecule inhibitors of these kinases. We report here the discovery of one such compound, amlexanox, which had previously been developed for the treatment of asthma, allergic rhinitis, and aphthous ulcers, but with an unclear mechanism of action [20, 21]. Administration of this selective TBK1/IKKε inhibitor to obese mice produces reversible weight loss, improved insulin sensitivity, reduced inflammation and attenuated hepatic steatosis, without affecting food intake. These data suggest that IKKε and TBK1 are part of a counter-inflammatory process that sustains energy storage in the face of insulin resistance [22]. Disruption of this process by amlexanox thus increases adaptive energy expenditure and restores insulin sensitivity. Because of the apparent safety of this drug in patients, we propose that it undergo study for the treatment of obesity, type 2 diabetes and nonalcoholic fatty liver disease in patients.

Results

Obesity increases IKKε and TBK1 activity in liver and fat through NF-κB

In a previous study [15], we reported that mRNA levels of both *Ikbke* and *Tbk1* are elevated in white adipose tissue (WAT) from HFD-fed mice as compared to normal diet (ND) controls, while *Ikbke* mRNA is elevated in liver. Immune complex assays revealed that both IKKε and TBK1 kinase activity were elevated in livers from HFD-fed mice (Fig. 1a). In the adipose tissue, we also observed higher kinase activity, even when normalized to the elevated protein levels. This increased expression was observed at six to seven weeks of

HFD, directly correlating with the onset of inflammatory macrophage infiltration in adipose tissue and liver (data not shown).

We modeled inflammation in 3T3-L1 cells by treating differentiated adipocytes with the inflammatory cytokine TNF-α [23]. Chronic TNF-α treatment increased mRNA levels of both kinases (Fig. 1b). These effects were prevented by pretreatment of cells with the IKKβ inhibitor compound VIII [24]. Furthermore, TNF-α produced a dose-dependent increase in IKKε protein levels in these cells, along with the down regulation of PPARγ. TNF-α also produced increased phosphorylation of TBK1 at Ser172, associated with activation (Fig. 1c).

To investigate whether inflammatory signals are responsible for induction of these kinases *in vivo*, we treated HFD-fed mice with the PPARγ agonist rosiglitazone, and the ω-3 fatty acid GPR120 agonists, EPA and DHA. Both substances reduce the inflammation and insulin resistance associated with obesity [25]. ω-3 fatty acid treatment markedly attenuated the HFD-induced elevation in the expression of IKKε mRNA and protein levels in both WAT and liver (Fig. 1d,e). Treatment of obese mice with rosiglitazone also reduced expression of *Ikbke* in adipocytes as well as in the stromal vascular fraction of WAT (Fig. 1f). Because neither rosiglitazone nor ω-3 fatty acid-treated animals lose weight [25], the elevated expression of these kinases from high fat feeding must be the result of inflammation, rather than a direct result of obesity.

Amlexanox is a specific inhibitor of IKKε and TBK1

Since deletion of the *Ikbke* gene in mice produced partial resistance to the effects of HFD [15], we screened a library of 150,000 chemical compounds to search for inhibitors of IKKε, using recombinant baculoviral expressed, purified full length IKKε, with MBP as a substrate, and identified amlexanox as a high affinity inhibitor (Fig. 2a). This previously discovered drug of unknown mechanism is used to treat asthma and allergic rhinitis in Japan and aphthous ulcers in the US [20, 21].

Dose response experiments revealed that amlexanox blocked IKKε activity with a half maximal inhibitory concentration of approximately 1–2 μM (Fig. 2b). It also blocked the activity of TBK1 at approximately the same concentrations, but was without effect on IKKα or β, and at these concentrations did not block any others from a broad panel of kinases representing most families. TBK1 and IKKε share overall 65% sequence similarity, and are 72% identical in the ATP binding region. Inhibition of IKKε or TBK1 (data not shown) by amlexanox was competitive for its substrate ATP (Fig. 2c), indicating that it interacts with the enzymes in the ATP-binding site. This is consistent with a model of the compound docked in the presumed ATP binding pocket of TBK1 (Fig. 2d), based on its published structure [26].

Amlexanox increased phosphorylation of TBK1 on Ser172 in 3T3-L1 adipocytes, and blocked polyinosinic:polycytidylic acid (poly I:C)-stimulated phosphorylation of interferon responsive factor-3 (IRF3), a presumed substrate of IKKε and TBK1 [27] (Fig. 2e). Reduced IRF3 phosphorylation was also produced by the previously identified IKKε/TBK1 inhibitor Cay-10576 (cayman) [28]. Furthermore, cayman treatment of RAW264.7 macrophages stimulated with lipopolysaccharide (LPS) or poly I:C also blocked the phosphorylation of

IRF3, and stimulated phosphorylation of TBK1 on Ser172 (Fig. 2f). This increased phosphorylation of TBK1 was also observed in peritoneal macrophages derived from *Ikbke* knockout (KO) mice (data not shown), and is likely due to blockade of feedback inhibition of the pathway [29], as evidenced by higher IKKβ phosphorylation in cayman-treated RAW cells.

Amlexanox produces reversible weight loss in obese mice

We fed C57Bl/6 mice a diet of 45% fat, and gavaged them daily with a vehicle control, 25 or 100 mg per kg amlexanox, while monitoring body weight (Fig. 3a). Serum concentrations of the drug exceed 5 μM at these doses [30]. Treatment of animals with either dose of amlexanox prevented the weight gain produced by HFD; drug-treated mice maintained weights equivalent to those of vehicle-treated control diet mice throughout 12 weeks. There was no effect of the drug on food intake, either at the beginning or end of the study (Fig. 3b).

We also evaluated amlexanox in mice with established obesity (Fig. 3c, supplementary Fig. 1, online). Amlexanox produced a 10 gram weight loss in HFD-fed obese mice after only four weeks of treatment, with no further effect thereafter. Moreover, escalation of the dose at this point was without further effect on weight (data not shown). Withdrawal of the drug after eight weeks of treatment restored weight gain, which returned to control weights after six to eight weeks. Weight loss during the treatment phase was accompanied by more than a 6 gram reduction in overall mass of adipose tissue, as well as an 80% decrease in fasting leptin concentration, whereas serum triglycerides, free fatty acids and cholesterol were unchanged (Fig. 3d and data not shown).

To determine whether the effects of amlexanox could be seen in another model of obesity, we treated ob/ob mice [31, 32] with 100 mg per kg of amlexanox or vehicle control, and monitored body weight (Fig. 3e). Although the drug had no effect on food intake, amlexanox produced a seven to eight gram weight loss after four weeks of treatment. Amlexanox also caused a significant decrease in adipose tissue mass in these mice, and an increase in circulating adiponectin (Fig. 3f,g).

Because there was no effect of amlexanox on food intake, we reasoned that the weight loss was due to increased energy expenditure. We thus used metabolic cages to monitor energy expenditure in diet-induced obese (DIO) mice treated with or without the drug. Four-week treatment of DIO mice with 25 mg per kg amlexanox resulted in significantly higher oxygen consumption as compared to vehicle control, consistent with an increase in energy expenditure (Fig. 3h). Exhaled carbon dioxide was also significantly higher, such that the respiratory exchange ratio remained unchanged compared to control-treated mice (Supplementary Fig. 2, online). Amlexanox had no effect on ND-fed mice, in which neither IKKε nor TBK1 is induced, suggesting that amlexanox might induce an increase in thermogenesis. Amlexanox treatment produced an approximate one degree increase in body temperature compared to HFD vehicle-treated mice, restoring the temperatures to levels observed in ND mice (Fig. 3i).

Amlexanox improves insulin sensitivity in obese mice

To assess in more detail the metabolic impact of amlexanox treatment, we treated DIO mice with 25 mg per kg amlexanox or vehicle control for eight weeks either before or after obesity was established, followed by assessment of metabolic parameters. Mice treated with amlexanox concurrently with HFD had improved glucose tolerance, with an approximate 30–40% reduction in the area under the curve for glucose (Fig. 4a). Treatment of mice with amlexanox after established DIO reversed elevations in fasting serum insulin caused by HFD, suggesting improved insulin sensitivity (Fig. 4b). Insulin tolerance tests revealed that amlexanox significantly improved insulin sensitivity in mice with established DIO, as indicated by a restoration in insulin responsiveness to ND levels (Fig. 4c and Supplementary Fig 3a, online). The drug did not affect insulin sensitivity in ND-fed mice. After four weeks of treatment, amlexanox produced marked improvements in glucose (Fig. 4d) and insulin tolerance (Fig. 4e and Supplementary Fig 3b, online) in ob/ob mice. Taken together, these effects are comparable to what is observed with established insulin sensitizing drugs such as the thiazolidinediones [33], suggesting that amlexanox is a *bona fide* insulin sensitizer.

We used hyperinsulinemic euglycemic clamp studies to investigate the tissue-specific effects of amlexanox on insulin sensitivity. Consistent with improved overall insulin sensitivity, the glucose infusion rate was significantly higher in amlexanox-treated animals (Fig. 4f and Supplementary Fig 3c, online). Insulin-mediated suppression of hepatic glucose production was dramatically enhanced by amlexanox treatment (Fig 4g). However, no change in glucose turnover rate was observed (Fig. 4h). Amlexanox treatment had no effect on glucose handling in ND-fed mice (Supplementary Fig 3d–g, online). These results indicate that the liver is an important target of amlexanox in mediating improved insulin sensitivity. Furthermore, these results support the action of amlexanox through IKKε/TBK1, both of which are induced in the liver by HFD. Amlexanox-treated mice exhibit enhanced insulin-mediated suppression of serum free fatty acids, indicative of increased suppression of adipose tissue lipolysis (Fig. 4i). Moreover, while basal phosphorylation of HSL was higher in adipose tissue from amlexanox-treated mice, the dephosphorylation of HSL produced by insulin was enhanced after amlexanox treatment compared to vehicle-treated mice on HFD (Supplementary Fig. 3h, online). Phosphorylation of Akt in response to insulin was also enhanced in amlexanox-treated mice compared to vehicle controls, indicating improved insulin sensitivity in WAT (Supplementary Fig. 3i, online).

Amlexanox reverses hepatic steatosis in obese mice

We treated DIO mice with 25 mg per kg amlexanox or vehicle control for eight weeks, and examined their livers post mortem (Fig. 5a). The hepatomegaly normally observed in high fat fed mice was largely reversed by the drug, with a greater than 20% reduction in liver weight (Fig. 5b). Moreover, triglyceride content in liver was reduced more than 50% in the amlexanox-treated mice compared to vehicle control. Hepatic glycogen content, which is elevated in HFD-fed mice, was reduced by amlexanox (Fig. 5c). Large lipid droplets were apparent by H&E staining in livers from control DIO mice, but were largely disseminated by amlexanox, consistent with the major reduction in triglycerides, glycogen and liver weight (Fig. 5d). These beneficial reductions in hepatic lipids were reversed in livers from mice that

were taken off drug and continued on HFD (Fig. 5e). Steatosis was also resolved in ob/ob mice treated with the drug (Supplementary Fig. 4a–c, online).

To further investigate the hepatosteatotic phenotype, we measured the expression of key metabolic and inflammatory genes in the livers of ND, HFD, and amlexanox-treated HFD mice. Amlexanox treatment reduced the expression of certain key lipogenic genes compared to HFD control mice, including fatty acid synthase (*Fasn*), malic enzyme 1 (*Me1*), acetyl CoA carboxylase (*Acaca*), and stearyl CoA desaturase 1 (*Scd1*) (Fig. 5f). Indicative of increased lipid load, HFD promoted the expression of *Ppara*, *Pparg*, *Cd36*, fatty acid binding protein 4 (*Fabp4*) and lipoprotein lipase (*Lpl*). Amlexanox lowered the expression of these genes towards ND levels. Gluconeogenic gene expression was modestly elevated by HFD; amlexanox did not significantly reduce gluconeogenic gene expression, but did lower the HFD-induced expression of glycolytic genes (Fig. 5g). In addition, a reduction in the HFD-induced expression of several inflammatory genes was observed, including the proinflammatory cytokines *Tnfa*, *Cxcl10*, and *Ccl*5 (Rantes) (Fig. 5h), the chemotactic factors *Ccl2* (Mcp1) and *Ccl3* (Mip-1α), and markers of macrophage infiltration, such as *Emr1* and *Itgax* (F4/80 and Cd11c). Expression of cytochrome b-245, β-polypeptide (*Cybb*), which is involved in the microbicidal oxidase system of phagocytes, was also lowered by drug treatment. Genetic measures of hepatosteatosis were similarly reduced in ob/ob mice (Supplementary Fig. 4d,e, online).

Amlexanox reduces chronic adipose tissue inflammation in obese mice

Amlexanox treatment markedly reduced the infiltration of inflammatory macrophages in white adipose tissue compared to vehicle-treated mice, as assessed by H&E staining (Fig. 6a). This amlexanox-dependent reduction in the appearance of macrophages in crown-like structures [34] was accompanied by a marked attenuation in the levels of mRNAs encoding key inflammatory genes in adipose tissue, including *Tnfa*, *Ccl2*, *Ccl3*, *Itgax*, and *Emr1* (Fig. 6b). We also measured the concentration of cytokines in the serum of control and amlexanox-treated mice. While there was no effect of the drug on circulating concentrations levels of Mcp1 or Rantes, TNF-α, IL-1α and Mip-1α were reduced (Fig. 6c). Serum concentrations of the anti-inflammatory cytokine, IL-10 [35], were elevated in amlexanox-treated mice compared to controls. Higher expression of fat cell-enriched proteins such as *Slc2a4* and *Pparg*, which are indicative of improved insulin sensitivity, was observed in WAT from amlexanox-treated mice (Fig. 6b). The levels of UCP-1 protein were also higher in the adipose tissue of amlexanox-treated DIO mice as compared to HFD vehicle-treated controls (Fig. 6d).

To evaluate whether amlexanox might control energy metabolism by directly affecting inflammation, we examined the effects of the drug on primary macrophages or the cultured RAW267.2 macrophage cell line. Addition of amlexanox did not affect macrophage migration in a wound-healing assay performed in RAW267.2 cells (Supplementary Fig. 5a, online). Bone marrow-derived and peritoneal macrophages from *Ikbke* KO mice were slightly more responsive to the effects of LPS in inducing the expression of various cytokines (Supplementary Fig. 5b–d, online). We also evaluated the effect of these inhibitors on poly I:C or TNF-α-stimulated NF-κB activation in adipocytes, and observed a slight

increase in the activation of NF-κB after pre-treatment with the IKKε/TBK1inhibitors (Supplementary Fig. 5e, online). Moreover, bone marrow transplant from *Ikbke*-deficient into wildtype mice on HFD did not influence weight or insulin sensitivity (data not shown). Together with the increase in TBK1 phosphorylation induced by the inhibitors described in Figure 2, these data indicate that inhibition of IKKε/TBK1 does not directly block the pro-inflammatory effects of cytokines or LPS on inflammatory signaling or the NF-κB pathway, but may rather prevent feedback inhibition that is a consequence of elevated expression of TBK1 and IKKε. Thus, these noncanonical kinases do not act as IκB kinases, and are not directly pro-inflammatory. However, IKKε and TBK1 may attenuate, without eliminating, the inflammatory response. Thus, the induction of these "counter-inflammatory" kinases may contribute to the generation of low-grade, sustained inflammation in obesity by preventing its resolution.

Amlexanox promotes energy expenditure in adipose tissue

In order to discern whether amlexanox directly influences phosphorylation *in vivo*, we first examined a number of proteins known to undergo hyperphosphorylation in states of obesity. As previously described [36], phosphorylation of proteins in the mTORC1 pathway such as S6K and S6 were elevated in response to HFD; this increase was largely attenuated in amlexanox-treated DIO mice (Fig. 6d and Supplementary Fig. 6a,b, online). The drug also blocked HFD induction of IKKε and TBK1 protein in adipose tissue. This finding was consistent with the fact that overexpression of wildtype but not kinase-inactive TBK1 in cells enhanced the stimulation of S6K phosphorylation by insulin, while knockdown of *Ikbke* or *Tbk1* in 3T3-L1 adipocytes lowered insulin-stimulated rS6 phosphorylation (Supplementary Fig. 6c, online). In adipose tissue from HFD-fed mice, hormone sensitive lipase (HSL) phosphorylation was lower, consistent with the well-established desensitization of the β-adrenergic pathway in this tissue during obesity [37]. Amlexanox treatment prevented the reduction in HSL phosphorylation associated with HFD (Fig. 6d and Supplementary Fig. 6a,b, online).

In control-treated mice on HFD, brown adipose tissue accumulated large lipid droplets, and acquired some of the features of white fat. Brown fat reverted to its normal appearance in amlexanox-treated mice (Supplementary Fig. 6d, online), with a corresponding reversal of HFD-induced triglyceride accumulation (Supplementary Fig. 6e, online). After withdrawal of amlexanox, lipids again accumulated in the BAT, reverting to the HFD phenotype of control obese mice (Supplementary Fig. 6f, online). UCP1 protein levels were also significantly elevated in the BAT of amlexanox treated mice (Fig. 5e and Supplementary Fig. 6g, online). Expression of the brown fat-specific markers *Prdm16*, *Ppargc1a*, *Ppargc1b*, *Cidea* and *Ucp1* were higher in amlexanox-treated mice (Fig. 6f). There was also an increase in the expression of cytochrome oxidases and *Elovl3*, which are involved in lipid metabolism in the BAT. Amlexanox treatment reduced IKKε and TBK1 protein levels in BAT (Fig. 6g and Supplementary Fig. 6h, online). Reduced signaling through the mTORC1 pathway was also observed in BAT of amlexanox-treated mice as compared to controls. *Ex vivo* treatment with amlexanox acutely stimulated lipid oxidation and oxygen consumption in BAT explants from HFD-fed animals, supporting a direct effect of amlexanox on energy expenditure (Fig. 6h,i).

To evaluate the roles of IKKε and TBK1 in mediating the effects of the drug, we treated *Ikbke* KO mice with amlexanox, and monitored weight loss and insulin sensitivity. Weight loss produced by amlexanox was equivalent between wildtype and *Ikbke* KO mice, indicating that the upregulation of TBK1 in these mice may compensate for IKKε inhibition (Supplementary Fig. 7a, online). We also monitored insulin sensitivity by intermittent insulin tolerance tests over several weeks of treatment (Supplementary Fig. 7b, online). While *Ikbke* KO mice were more insulin sensitive than their wildtype littermates, the drug produced an additional improvement, achieving insulin sensitivity observed in WT mice treated with amlexanox. Improvements in insulin sensitivity preceded weight loss, indicating that improved insulin sensitivity may not be secondary to weight loss.

Since *Tbk1* knockout mice are not viable, we used mouse embryonic fibroblasts (MEFs) to further investigate the importance of these kinases in the specificity of amlexanox. Treatment of wildtype MEFs with amlexanox produced a dose-dependent increase in the phosphorylation of TBK1 and the P65 NF-κB subunit, presumably due to feedback inhibition [27]. Both effects were absent in *Ikbke*/*Tbk1* double KO MEFs (Supplementary Fig. 7c–e, online). However, single KO MEFs retained responsiveness to amlexanox. In *Ikbke* KO MEFs, we observed TBK1 phosphorylation and degradation of IκBα after amlexanox treatment, while *Tbk1* KO MEFs exhibited a robust phosphorylation of IKKβ in response to amlexanox treatment. Amlexanox also enhanced oxygen consumption in wildtype but not *Ikbke*/*Tbk1* double KO MEFs, indicating that the energy expenditure-promoting effect of amlexanox is mediated specifically through inhibition of both IKKε and TBK1 (Fig. 6j). Taken together, these data suggest that amlexanox elicits it effects though specific inhibition of both IKKε and TBK1.

Discussion

Compelling evidence has accrued over the past few years that both genetic and dietary forms of rodent obesity are accompanied by the generation of low-grade inflammation in adipose and liver tissue that serves as a key link between obesity and sustained insulin resistance [7–11]. Almost all rodent models of obese insulin resistance are associated with chronic inflammation, and there has been a strong correlation between insulin resistance and inflammatory markers in studies of several patient groups [38–41]. This inflammation is generally low-grade, and accompanied by macrophage switching from a Type 2 to Type 1 polarization state [35, 42, 43], as well as the presence of additional inflammatory cells [44–47]. Inhibition of inflammatory signaling by knockout of key pathways in obese mice can disrupt the link between obesity and insulin resistance [11, 48–55]. Likewise, different anti-inflammatory pharmacological and genetic approaches can also reduce insulin resistance in rodents and patients [56–58]. Co-culture studies and neutralizing antibodies directed against different proinflammatory cytokines have demonstrated *in vitro* that inflammatory signals derived from M1-polarized macrophages can desensitize cells to insulin via different mechanisms [23].

While the molecular links between inflammation and insulin resistance are not yet completely understood, it is clear that the NF-κB program plays a key role [13]. Disruption of NF-κB signaling via targeted knockout of the canonical IκB kinase IKKβ gene or

pharmacological inhibition of this pathway can restore insulin sensitivity in obese states. However, the roles of the noncanonical IKKs, TBK1 and IKKε, in this process are less well understood. Our previous studies indicated that deletion of the IKKε gene partially restored insulin sensitivity and reduced weight in animals fed HFD, despite having no apparent effect on NF-κB signaling, although the relevant mechanism was not defined [15]. In this report we describe amlexanox, a novel chemical inhibitor of IKKε and TBK1, that reproduces many of these effects. Administration of this compound to mice reduces weight, insulin resistance, inflammation and steatosis in three different obese mouse models. These effects are seen within three to four weeks after starting drug therapy, and are reversible. They are likely attributed to increased triglyceride hydrolysis and oxidation, along with reduced lipogenesis and glycogenesis. Signaling pathways that modulate these processes are attenuated *in vitro* by addition of amlexanox or another structurally unrelated inhibitor to cultured adipocytes.

The precise mechanisms by which amlexanox produces these beneficial effects in obese rodents remain to be completely elucidated. While amlexanox is known to be a mast cell stabilizer of unknown mechanism [20], and depletion of mast cells may have beneficial metabolic effects [59], most of the *in vivo* and *in vitro* evidence points to a role for the drug in increasing expenditure of energy while reducing its storage in adipocytes and hepatocytes. Furthermore, the lack of a phenotype in WT mice reconstituted with IKKε KO bone marrow indicates that the role of IKKε in bone marrow-derived cells such as mast cells and macrophages is less important than its role in other cell types such as adipocytes and hepatocytes. While IKKε and TBK1 are elevated as part of the inflammatory program downstream of NF-κB, the kinase targets of the drug do not appear to be direct participants in the increased inflammatory program. In fact, the reduced inflammation observed *in vivo* with amlexanox treatment may be an indirect effect of improved metabolic disease, or perhaps elimination of a feedback pathway that maintains inflammation at low levels, such that inflammation is permitted to resolve. Moreover, despite the fact that administration of amlexanox to obese mice restores insulin sensitivity, these compounds are not direct insulin sensitizers *in vitro*. Phosphorylation analyses indicate that IKKε and TBK1 may co-opt signaling pathways that drive energy conservation in the face of insulin resistance, ensuring that energy expenditure is kept in check by reducing HSL phosphorylation and UCP1 expression in adipose tissue, while also increasing mTOR signaling to drive lipogenesis and glycogen synthesis. Thus, together these data suggest that expression of TBK1 and IKKε by obesity-dependent inflammation may conserve energy during the transition from an insulin-dependent to an insulin-independent state of nutrient storage. Moreover, it is likely that the improvement in insulin resistance produced by treatment with the drug results from reducing excessive energy storage, while preventing homeostatic feedback loops (such as mTOR) that block insulin receptor signaling [60].

Amlexanox appears to be a relatively safe drug with a long history of use in patients. As such, there might be an interesting opportunity for repurposing this agent for diabetes and obesity. Future clinical studies will be needed to explore this possibility, and to validate the hypothesis that these noncanonical IκB kinases contribute to counter-inflammatory actions that sustain metabolic disease.

Materials and Methods

Reagents

All chemicals were obtained from Sigma-Aldrich unless otherwise stated. IKKε (2690), TBK1 (3013), phosphorylated TBK1 (Ser172-5483), IKKα/β (2684), phosphorylated IKKα/β (ser176-2687) AKT (9272), phosphorylated AKT (Ser473-9272), S6K(2708 diluted 1:250), phosphorylated S6K (Thr389-9205), S6 (2317), phosphorylated S6 (Ser235/236-2211), IRF3 (4302), phosphorylated IRF3 (Ser396-4947), HSL (4107), phosphorylated HSL (Ser563-4139 or Ser660-4126), and PPARγ (2443)-specific antibodies were purchased from Cell Signaling. RalA (610222)-specific antibody was obtained from BD Bioscience. UCP1 (UCP11-A-diluted 1:250 for WAT detection)-specific antibody was obtained from Alpha Diagnostics. All antibodies were diluted 1:1,000 unless otherwise noted. Enhanced chemiluminescence reagents were purchased from NEN, Inc. EDTA-free protease inhibitor tablet was purchased from Roche Diagnostics.

Animals and animal care

We fed wildtype male C57BL/6 mice a HFD consisting of 45% of calories from fat (D12451 Research Diets Inc.) starting at eight weeks of age for 12–24 weeks, while ND C57BL/6 controls were maintained on normal chow diet consisting of 4.5% fat (5002 Lab Diet). We fed C57BL/6 diets containing ω-3 fatty acids as previously described [25]. Rosiglitazone treatment was administered for three weeks by addition of the compound to the diet in mice that had been on HFD for 16 weeks. Each mouse consumed on average 3.5 mg per kg rosiglitazone per day. Amlexanox was administered by daily oral gavage. For the prevention groups, amlexanox (25 mg per kg or 100 mg per kg) administration was begun concurrently with HFD feeding at eight weeks of age. For the treatment groups, 25 mg per kg amlexanox treatment was begun at 20 weeks of age after 12 weeks of HFD. To test the effect of amlexanox withdrawal, mice in the treatment group were switched from amlexanox gavage to vehicle control after eight weeks of amlexanox treatment. We fed control and ob/ob mice a normal chow diet and gavaged with 100 mg per kg amlexanox or vehicle control beginning at ten weeks of age. Animals were housed in a specific pathogen-free facility with a 12-hour light/12-hour dark cycle and given free access to food and water. All animal use was in compliance with the Institute of Laboratory Animal Research Guide for the Care and Use of Laboratory Animals and approved by the University Committee on Use and Care of Animals at the University of Michigan and UCSD.

Food intake

The remaining weight of food provided was determined daily for singly housed mice. Daily food consumption was calculated from a three-day average.

Energy expenditure and respiratory quotient

C57Bl6 mice in the amlexanox treatment group were placed in metabolic cages. The University of Michigan Metabolic Phenotyping Core measured oxygen consumption (VO_2), carbon dioxide production (VCO_2) and spontaneous motor activity during 3 consecutive days using the Comprehensive Laboratory Monitoring System (Columbus Instruments), an

integrated open-circuit calorimeter equipped with an optical beam activity monitoring system [53]. Values presented are normalized to body weight. The respiratory quotient was calculated by dividing carbon dioxide production by oxygen consumption. We used the mean values for light and dark cycles to analyze statistical significance.

Body composition

The University of Michigan Metabolic Phenotyping Core used NMR analysis to quantify body fat, lean body mass and fluid content in ob/ob mice and C57BL/6 mice in the amlexanox treatment group.

Hyperinsulinemic Euglycemic clamp

C57Bl6 mice placed on HFD starting at eight weeks of age, starting at 16 weeks of age mice were gavaged daily with amlexanox or vehicle control. After four weeks of treatment, the right jugular vein and carotid artery were surgically catheterized and mice were given 5 days to recover from the surgery. During this recovery period, amlexanox was delivered in drinking water. On the day of the clamp a final oral gavage treatment was performed. After a 5–6 hour fast, hyperinsulinemic clamp studies were performed on conscious mice using the protocol adopted from the Vanderbilt Mouse Metabolic Phenotyping Center by the University of Michigan Animal Phenotyping Core consisting of a 90 min equilibration period, followed by a 120 min experimental period (t = 0 to 120 min). Insulin was infused at 4.0 mU kg^{-1} min^{-1}. This experiment was performed at the University of Michigan Metabolic Phenotyping Core. We measured serum free fatty acid levels using the colorimetric NEFA-HR(2) kit (Wako).

Core body temperature

We performed rectal temperature measurements using a YSI 4600 Precision thermometer (YSI, Inc.).

Blood chemistry analysis

Blood glucose was measured by OneTouch Ultra Glucometer. Plasma from mice fasted for six hours was isolated from whole blood collected into heparinized tubes. We used an insulin ELISA kit (Crystal Chem Inc.) to measure serum insulin concentrations. Leptin and adiponectin levels were measured by ELISA kits purchased from Cayman Chem Inc. We quantified serum cytokine levels using luminex technology in a multi-analyte panel plate purchased from Millipore. Additionally, we measured TNF-α levels using ELISA kits purchased from R&D Systems.

Glucose and insulin tolerance tests

For glucose tolerance tests, after a six-hour fast, we gavaged mice with glucose at a dose of 1.5 g per kg (C57BL/6 mice) or 1.2 g per kg (ob/ob mice). For insulin tolerance tests, mice were fasted for three hours then given an intraperitoneal injection of insulin (1.2 units per kg for C57BL/6 mice and 2.0 units per kg for ob/ob mice). We measured blood glucose at basal, 15, 30, 45, 60, 90, 120 and 180 minutes from tail blood using the OneTouch Ultra glucometer (Lifescan).

Tissue lipid content

We isolated liver lipids by ethanolic KOH saponification and BAT lipids by chloroform extraction and then triglyceride levels were quantified using the Triglyceride Reagent kit (Thermo Scientific).

Liver glycogen content

We digested liver tissue in a 30% potassium hydroxide solution, and then glycogen was precipitated using 70% ethanol. After three washes (resuspend pellet in water, then add ethanol to 70% and centrifuge down pellet) to remove any traces of glucose, we digested glycogen by addition of amyloglucosidase. Released glucose was quantified using a colorimetric kit (Wako).

Stromal vascular fraction (SVF) and adipocyte isolation

We digested excised WAT in PBS containing 1% BSA and 1mg mL^{-1} type II collagenase for 30 minutes at 37°C with gentle agitation. The cell suspension was filtered through a 100 μm filter and then centrifuged at 700 × *g* for 5 minutes to separate floating adipocytes from SVF pellet. We washed floating adipocytes twice with PBS containing 1% BSA and collected the SVF pellets after each wash.

Western analysis

We homogenized tissues in lysis buffer (50mM Tris, pH7.5, 5mM EDTA, 250mM sucrose, 1% NP40, 2mM DTT, 1mM sodium vanadate, 100mM NaF, 10mM $Na_4P_2O_7$, and freshly added protease inhibitor tablet), and then incubated them for one hour at 4 °C [15]. We centrifuged crude lysates at 14,000 × *g* for 15 minutes twice and determined the protein concentration using BioRad Protein Assay Reagent. Samples were diluted in sodium dodecyl sulfate (SDS) sample buffer. Bound proteins were resolved by SDS-polyacrylamide gel electrophoresis and transferred to nitrocellulose membranes (Bio-Rad). Individual proteins were detected with the specific antibodies and visualised on film using horseradish peroxidase-conjugated secondary antibodies (Bio-Rad) and Western Lightning Enhanced Chemiluminescence (Perkin Elmer Life Sciences). Alternatively, infrared fluorescent secondary antibodies were used for detection and quantification of specific protein on the Odyssey CLx imager (LI-COR).

Histochemistry

Tissues were fixed in formalin for 3 days. The University of Michigan Cancer Center Research Histology Laboratory performed histology. A 1:100 dilution of the UCP1 (UCP11-Alpha Diagnostics) specific antibody at 10 μg mL^{-1} was used for immunohistochemical detection of UCP1 protein.

Gene expression analysis

We rinsed isolated mouse tissues in phosphate buffered saline (PBS), then froze them in liquid nitrogen and stored them at −80 °C until extraction. We extracted total RNA from Liver, WAT and BAT tissues as well as differentiated 3T3-L1 cells using the RNeasy Lipid Tissue Kit (Qiagen) according to the manufacturer's instructions with the inclusion of a

DNase digestion step. We extracted total RNA from BMDM and SVF cells using the RNeasy Kit (Qiagen) with a DNase step. We used the Superscript First-Strand Synthesis System for RT-PCR (Invitrogen) with random primers for reverse transcription. Realtime (RT) PCR amplification of the cDNA was performed on samples in triplicate with Power SYBR Green PCR Master Mix (Applied Biosystems) using the Applied Biosystems 7900HT Fast RT-PCR System. We chose Adrp and GAPDH as the internal control for normalization after screening several candidate genes; their expression was not significantly affected by experimental conditions. Sequences of all primers used in this study are listed in Supplementary Table 2. Data was analyzed using the $2^{-\Delta\Delta CT}$ method, and the control sample value was normalized to 1. Other data was quantified using an internal standard curve. Statistical significance was determined using the unpaired heterocedastic Student's t-test with one averaged sample value per mouse.

Lipid oxidation rate

We excised intrascapular BAT and placed it in DMEM with 2% BSA with and without 50 μM amlexanox then incubated at 37 °C for 1 hour, after which we changed the media to DMEM with 2% BSA, 0.25 mM carnitine, 0.2 mM palmitic acid and trace levels of ^{3}H-palmitic acid and incubated for one more hour at 37 °C and then collected the media, and isolated the aqueous faction. Lipid oxidation was determined by the conversion of ^{3}H-palmitic acid to $^{3}H_2O$.

IKKε and TBK1 *in vitro* kinase assays

We performed *in vitro* kinase assays by incubating purified kinase (IKKε or TBK1) in kinase buffer containing 25 mM Tris (pH7.5), 10 mM MgCl2, 1 mM DTT, and 10 μM ATP for 30 minutes at 30 °C in the presence of 0.5 μCi γ-[^{32}P]-ATP and 1 μg MBP per sample as a substrate. We stopped the kinase reaction by adding 4x sodium dodecyl sulfate (SDS) sample buffer and boiling for 5 minutes at 95°C. Supernatants were resolved by SDS-polyacrylamide gel electrophoresis, transferred to nitrocellulose, and analyzed by autoradiography using a Typhoon 9410 phosphorimager (GE Lifesciences). We quantified the bands using ImageQuant.

IKKε and TBK1 immune-complex kinase assay

We collected liver and white adipose tissues from C57BL/6 mice on ND or HFD, and homogenized the tissues using a Dounce homogenizer with lysis buffer containing 50 mM Tris (pH7.5), 150 mM NaCl, 2 mM EDTA, 5 mM NaF, 25 mM β-glycerophosphate, 1 mM sodium orthovanadate, 10% glycerol, 1% TritonX-100, 1 mM DTT, and 1 mM PMSF in the presence of protease inhibitors (Roche Diagnostics). We incubated tissue cell lysates for 1 hour at 4 °C and cleared them by spinning at 13,000 rpm for 15 minutes at 4 °C in a table-top centrifuge. Each 1 mg of lysate was subjected to immunoprecipitation using 5 μl of rabbit-polyclonal antibody against TBK1 or IKKε for 1.5 hours at 4 °C. We harvested immunocomplexes by incubation with ProtA beads (Roche Diagnostics) for 2 hours at 4 °C. We washed immunoprecipitates once with lysis buffer and three times with wash buffer containing 20 mM Hepes (pH 7.4), 50 mM NaCl, 20 mM β-glycerophosphate, 1 mM sodium orthovanadate, 5 mM NaF, 10 mM $MgCl_2$, and 1 mM DTT. We performed an *in vitro*

kinase assay using the immunoprecipitated kinases as described above. Relative levels of MBP phosphorylation were detected by autoradiograph and normalized to the levels of IKKε or TBK1 kinase detected in the immunoprecipitate by immunoblotting.

Cell culture

3T3-L1 fibroblasts (American Type Culture Collection) were cultured in 10% neonatal calf serum in Dulbecco's modified Eagle medium (DMEM) for proliferation and 10% fetal bovine serum (FBS) in Dulbecco's modified Eagle medium (DMEM) for differentiation. We grew the cells to confluence, then induced differentiation two days later with 500 μM 3-Isobutyl-1-methylxanthine, 250 nM dexamethasone, and insulin (1 μg mL^{-1}) for three days, followed by insulin only treatment for two days. We routinely used cells within 7 days after completion of the differentiation process; and only used cultures in which >90% of cells displayed adipocyte morphology. We serum-starved 3T3-L1 adipocytes with 0.5% fetal bovine serum (FBS) in Dulbecco's modified Eagle medium (DMEM) prior to treatment. TNF-α ng mL^{-1} unless otherwise noted) were performed during the 24 hour prior to harvest, after pretreatment with IKKβ inhibitor compound VIII (EMD Biosciences) for 1 hour where indicated. We pre-treated 3T3-L1 adipocytes for 1 hour with amlexanox at the given concentrations, then treated them with 20 μg ml^{-1} of poly I:C for 1 hour. Alternatively, we treated 3T3-L1 adipocytes with 50 μM forskolin for 15 minutes, after a 30-minute amlexanox pretreatment. We treated cells with or without 10 nM of insulin for 15 minutes. We determined glycerol release into the supernatant (DMEM without phenol red) using a colorimetric assay. We serum starved RAW264.7 cells with 0.5% FBS DMEM media and pre-treated with or without Cay-10576 (Cayman Chemical). The cells were then treated with LPS (0.5 μg ml^{-1}) or poly I:C (50 μg ml^{-1}) for 1 hour. We harvested the cells for total RNA and analyzed them by RT-PCR. We also resolved cell lysates by SDS-PAGE and analyzed them by immunoblot using the indicated antibodies. Wildtype and *Ikbke*/*Tbk1* double knockout (DKO) and single knockout (SKO) MEFs were kindly provided by Dr. Shizuo Akira. Cells were cultured in DMEM with 10% FBS, and serum starved in 0.5% FBS for 12 hours prior to treatment. TNF-α treatment (50 ng mL^{-1}) was performed for 15 minutes at the end of two hour pretreatment with amlexanox.

Oxygen consumption rate

The Michigan Metabolic Phenotyping Core and Michigan Nutritional Obesity Research Center measured oxygen consumption in cells and *ex vivo* tissue using an extracellular flux analyzer; model XF24-3 (Seahorse Bioscience).

Molecular modeling of amlexanox in the TBK1 ATP binding site

We modeled amlexanox into the known structure of the TBK1 catalytic domain (PDB ID codes 4EUT and 4EUU and [26]). The best fit of amlexanox in the active site of TBK1 was obtained using AutoDock Vina.

Statistical Analyses

Averaged values are presented as the mean ± s.e.m. When comparing two groups, we determined statistical significance using the student's t-test. When more than two groups

were investigated, we first performed an ANOVA to establish that not all groups were equal. Following a statistically significant ANOVA, we performed between group comparisons using the Tukey-Krammer post-hoc analysis. ANOVA and Tukey-Krammer tests were performed using Stata version 12.0.

Supplementary Material

Refer to Web version on PubMed Central for supplementary material.

Acknowledgements

We thank J. Hung and X. Peng for excellent technical assistance, and members of the Saltiel laboratory for helpful discussions. This work was supported by US National Institutes of Health grants DK60597 and 60591 to A. Saltiel, F32DK09685101 to S. Reilly, F30DK089687 to J. Mowers, and R24DK090962 to A. Saltiel, J. Olefsky and R. Evans. We also acknowledge support from the Michigan Diabetes Research and Training Center (DK020572), Michigan Institute for Clinical and Health Research (UL1-RR024986), Nathan Shock Center, Michigan Metabolic Phenotyping Core and Michigan Nutritional Obesity Research Center (DK089503).

References

1. Taniguchi CM, Emanuelli B, Kahn CR. Critical nodes in signalling pathways: insights into insulin action. Nat Rev Mol Cell Biol. 2006; 7:85–96. [PubMed: 16493415]
2. Reaven GM. The insulin resistance syndrome: definition and dietary approaches to treatment. Annual review of nutrition. 2005; 25:391–406.
3. Reaven GM. Why Syndrome X? From Harold Himsworth to the insulin resistance syndrome. Cell metabolism. 2005; 1:9–14. [PubMed: 16054040]
4. Stumvoll M, Goldstein BJ, van Haeften TW. Type 2 diabetes: principles of pathogenesis and therapy. Lancet. 2005; 365:1333–1346. [PubMed: 15823385]
5. Biddinger SB, Kahn CR. From mice to men: insights into the insulin resistance syndromes. Annual review of physiology. 2006; 68:123–158.
6. Doria A, Patti ME, Kahn CR. The emerging genetic architecture of type 2 diabetes. Cell metabolism. 2008; 8:186–200. [PubMed: 18762020]
7. Olefsky JM, Glass CK. Macrophages, inflammation, and insulin resistance. Annual review of physiology. 2010; 72:219–246.
8. Li P, et al. Functional heterogeneity of CD11c-positive adipose tissue macrophages in diet-induced obese mice. The Journal of biological chemistry. 2010; 285:15333–15345. [PubMed: 20308074]
9. Lumeng CN, Saltiel AR. Inflammatory links between obesity and metabolic disease. The Journal of clinical investigation. 2011; 121:2111–2117. [PubMed: 21633179]
10. Gregor MF, Hotamisligil GS. Inflammatory mechanisms in obesity. Annual review of immunology. 2011; 29:415–445.
11. Hotamisligil GS. Endoplasmic reticulum stress and the inflammatory basis of metabolic disease. Cell. 2010; 140:900–917. [PubMed: 20303879]
12. Wunderlich FT, et al. Hepatic NF-kappa B essential modulator deficiency prevents obesity-induced insulin resistance but synergizes with high-fat feeding in tumorigenesis. Proceedings of the National Academy of Sciences of the United States of America. 2008; 105:1297–1302. [PubMed: 18216263]
13. Arkan MC, et al. IKK-beta links inflammation to obesity-induced insulin resistance. Nat Med. 2005; 11:191–198. [PubMed: 15685170]
14. Goldfine AB, et al. The effects of salsalate on glycemic control in patients with type 2 diabetes: a randomized trial. Annals of internal medicine. 2010; 152:346–357. [PubMed: 20231565]
15. Chiang SH, et al. The protein kinase IKKepsilon regulates energy balance in obese mice. Cell. 2009; 138:961–975. [PubMed: 19737522]

16. Chau TL, et al. Are the IKKs and IKK-related kinases TBK1 and IKK-epsilon similarly activated? Trends Biochem Sci. 2008; 33:171–180. [PubMed: 18353649]
17. Chariot A. The NF-kappaB-independent functions of IKK subunits in immunity and cancer. Trends in Cell Biology. 2009; 19:404–413. [PubMed: 19648011]
18. Kawai T, Akira S. Signaling to NF-kappaB by Toll-like receptors. Trends in molecular medicine. 2007; 13:460–469. [PubMed: 18029230]
19. Kravchenko VV, Mathison JC, Schwamborn K, Mercurio F, Ulevitch RJ. IKKi/IKKepsilon plays a key role in integrating signals induced by pro-inflammatory stimuli. The Journal of biological chemistry. 2003; 278:26612–26619. [PubMed: 12736252]
20. Makino H, Saijo T, Ashida Y, Kuriki H, Maki Y. Mechanism of action of an antiallergic agent, amlexanox (AA-673), in inhibiting histamine release from mast cells. Acceleration of cAMP generation and inhibition of phosphodiesterase. International archives of allergy and applied immunology. 1987; 82:66–71. [PubMed: 2433225]
21. Bell J. Amlexanox for the treatment of recurrent aphthous ulcers. Clinical drug investigation. 2005; 25:555–566. [PubMed: 17532700]
22. Saltiel AR. Insulin resistance in the defense against obesity. Cell metabolism. 2012; 15:798–804. [PubMed: 22682220]
23. Lumeng CN, Deyoung SM, Saltiel AR. Macrophages block insulin action in adipocytes by altering expression of signaling and glucose transport proteins. Am J Physiol Endocrinol Metab. 2007; 292:E166–E174. [PubMed: 16926380]
24. Karin M, Yamamoto Y, Wang QM. The IKK NF-kappa B system: a treasure trove for drug development. Nature reviews. Drug discovery. 2004; 3:17–26. [PubMed: 14708018]
25. Oh DY, et al. GPR120 is an omega-3 fatty acid receptor mediating potent anti-inflammatory and insulin-sensitizing effects. Cell. 2010; 142:687–698. [PubMed: 20813258]
26. Ma X, et al. Molecular basis of Tank-binding kinase 1 activation by transautophosphorylation. Proc Natl Acad Sci U S A. 2012; 109:9378–9383. [PubMed: 22619329]
27. Clark K, Takeuchi O, Akira S, Cohen P. The TRAF-associated protein TANK facilitates cross-talk within the IkappaB kinase family during Toll-like receptor signaling. Proc Natl Acad Sci U S A. 2011; 108:17093–17098. [PubMed: 21949249]
28. Bamborough P, et al. 5-(1H-Benzimidazol-1-yl)-3-alkoxy-2-thiophenecarbonitriles as potent, selective, inhibitors of IKK-epsilon kinase. Bioorganic & medicinal chemistry letters. 2006; 16:6236–6240. [PubMed: 16997559]
29. Clark K, et al. Novel cross-talk within the IKK family controls innate immunity. The Biochemical journal. 2011; 434:93–104. [PubMed: 21138416]
30. Torii H, et al. Metabolic fate of amoxanox (AA-673), a new antiallergic agent, in rats, mice, guinea-pigs and dogs. Japanese Pharmacology & Therapeutics. 1985; 13:4933–4954.
31. Friedman JM. Modern science versus the stigma of obesity. Nature medicine. 2004; 10:563–569.
32. Friedman JM, Halaas JL. Leptin and the regulation of body weight in mammals. Nature. 1998; 395:763–770. [PubMed: 9796811]
33. Olefsky JM, Saltiel AR. PPAR gamma and the treatment of insulin resistance. Trends Endocrinol Metab. 2000; 11:362–368. [PubMed: 11042466]
34. Weisberg SP, et al. Obesity is associated with macrophage accumulation in adipose tissue. J Clin Invest. 2003; 112:1796–1808. [PubMed: 14679176]
35. Lumeng CN, Bodzin JL, Saltiel AR. Obesity induces a phenotypic switch in adipose tissue macrophage polarization. J Clin Invest. 2007; 117:175–184. [PubMed: 17200717]
36. Um SH, et al. Absence of S6K1 protects against age- and diet-induced obesity while enhancing insulin sensitivity. Nature. 2004; 431:200–205. [PubMed: 15306821]
37. Seals DR, Bell C. Chronic sympathetic activation: consequence and cause of age-associated obesity? Diabetes. 2004; 53:276–284. [PubMed: 14747276]
38. Pradhan AD, Manson JE, Rifai N, Buring JE, Ridker PM. C-reactive protein, interleukin 6, and risk of developing type 2 diabetes mellitus. JAMA : the journal of the American Medical Association. 2001; 286:327–334. [PubMed: 11466099]

39. Festa A, D'Agostino R Jr, Tracy RP, Haffner SM. Elevated levels of acute-phase proteins and plasminogen activator inhibitor-1 predict the development of type 2 diabetes: the insulin resistance atherosclerosis study. Diabetes. 2002; 51:1131–1137. [PubMed: 11916936]
40. Blackburn P, et al. Postprandial variations of plasma inflammatory markers in abdominally obese men. Obesity. 2006; 14:1747–1754. [PubMed: 17062804]
41. Aron-Wisnewsky J, et al. Human adipose tissue macrophages: m1 and m2 cell surface markers in subcutaneous and omental depots and after weight loss. The Journal of clinical endocrinology and metabolism. 2009; 94:4619–4623. [PubMed: 19837929]
42. Schenk S, Saberi M, Olefsky JM. Insulin sensitivity: modulation by nutrients and inflammation. The Journal of clinical investigation. 2008; 118:2992–3002. [PubMed: 18769626]
43. Odegaard JI, Chawla A. Alternative macrophage activation and metabolism. Annual review of pathology. 2011; 6:275–297.
44. Nishimura S, et al. CD8+ effector T cells contribute to macrophage recruitment and adipose tissue inflammation in obesity. Nature medicine. 2009; 15:914–920.
45. Winer S, et al. Normalization of obesity-associated insulin resistance through immunotherapy. Nature medicine. 2009; 15:921–929.
46. Feuerer M, et al. Lean, but not obese, fat is enriched for a unique population of regulatory T cells that affect metabolic parameters. Nature medicine. 2009; 15:930–939.
47. Winer DA, et al. B cells promote insulin resistance through modulation of T cells and production of pathogenic IgG antibodies. Nature medicine. 2011; 17:610–617.
48. Nakamura T, et al. Double-stranded RNA-dependent protein kinase links pathogen sensing with stress and metabolic homeostasis. Cell. 2010; 140:338–348. [PubMed: 20144759]
49. Summers SA. Sphingolipids and insulin resistance: the five Ws. Current opinion in lipidology. 2010; 21:128–135. [PubMed: 20216312]
50. Vandanmagsar B, et al. The NLRP3 inflammasome instigates obesity-induced inflammation and insulin resistance. Nature medicine. 2011; 17:179–188.
51. Saberi M, et al. Hematopoietic cell-specific deletion of toll-like receptor 4 ameliorates hepatic and adipose tissue insulin resistance in high-fat-fed mice. Cell metabolism. 2009; 10:419–429. [PubMed: 19883619]
52. Wellen KE, et al. Coordinated regulation of nutrient and inflammatory responses by STAMP2 is essential for metabolic homeostasis. Cell. 2007; 129:537–548. [PubMed: 17482547]
53. Lesniewski LA, et al. Bone marrow-specific Cap gene deletion protects against high-fat diet-induced insulin resistance. Nat Med. 2007; 13:455–462. [PubMed: 17351624]
54. Holland WL, et al. Inhibition of ceramide synthesis ameliorates glucocorticoid-, saturated-fat-, and obesity-induced insulin resistance. Cell metabolism. 2007; 5:167–179. [PubMed: 17339025]
55. Shi H, et al. TLR4 links innate immunity and fatty acid-induced insulin resistance. The Journal of clinical investigation. 2006; 116:3015–3025. [PubMed: 17053832]
56. Solomon DH, et al. Association between disease-modifying antirheumatic drugs and diabetes risk in patients with rheumatoid arthritis and psoriasis. Jama. 2011; 305:2525–2531. [PubMed: 21693740]
57. Hundal RS, et al. Mechanism by which high-dose aspirin improves glucose metabolism in type 2 diabetes. The Journal of clinical investigation. 2002; 109:1321–1326. [PubMed: 12021247]
58. Zhang X, et al. Selective inactivation of c-Jun NH2-terminal kinase in adipose tissue protects against diet-induced obesity and improves insulin sensitivity in both liver and skeletal muscle in mice. Diabetes. 2011; 60:486–495. [PubMed: 21270260]
59. Liu J, et al. Genetic deficiency and pharmacological stabilization of mast cells reduce diet-induced obesity and diabetes in mice. Nature medicine. 2009; 15:940–945.
60. Zick Y. Ser/Thr phosphorylation of IRS proteins: a molecular basis for insulin resistance. Science's STKE : signal transduction knowledge environment. 2005; 2005:pe4. [PubMed: 15671481]

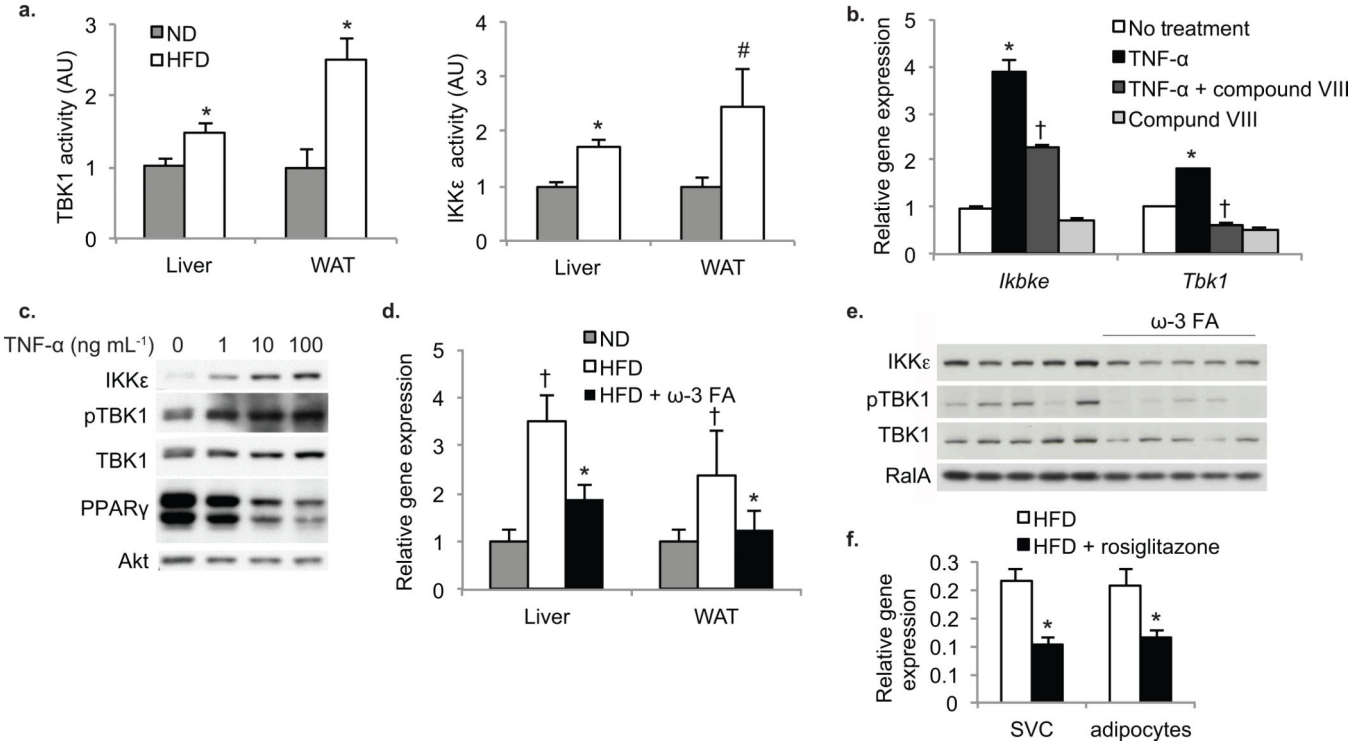

Figure 1. Induction of IKKε and TBK1 in obese mice is a result of increased inflammation

(**a**) TBK1 (left panel) and IKKε (right panel) activity in liver and WAT of mice fed ND (grey bars) or HFD (white bars). (*n*=4 per group). * *P* value < 0.05 ND versus HFD; # *P* value < 0.1 ND versus HFD. (**b**) Expression of *Ikbke* and *Tbk1* in differentiated 3T3-L1 cells without treatment (white bars), treated with TNF-α (black bars), compound VIII (light grey bars) or both TNF-α and compound VIII (dark grey bars). Results are representative of multiple experiments. * *P* value < 0.05 no treatment versus TNF-α only treatment. † *P* value < 0.05 TNF-α versus TNF-α + compound VIII. (**c**) IKKε, TBK1 and PPARγ protein levels and TBK1 phosphorylation at Ser172 after TNF-α treatment. Results were replicated in more than three experiments. Akt is a loading control. (**d**) *Ikbke* expression in liver and WAT of mice on ND (grey bars) or HFD with (black bars) and without (white bars) ω-3 fatty acids (FA). † *P* value < 0.05 ND versus HFD. * *P* value < 0.05 HFD versus HFD + ω-3 FA. (*n*=9 per group). (**e**) IKKε protein levels and TBK1 phosphorylation at Ser172 in HFD mice with and without ω-3 FA. RalA is a loading control. (**f**) *Ikbke* expression levels in adipocytes and stromal vascular fraction of mice fed HFD (white bars) or HFD plus rosiglitazone (black bars). * *P* value <0.05 HFD versus HFD plus rosiglitazone. (*n*=8 in HFD group, *n*=4 in HFD plus rosiglitazone group).

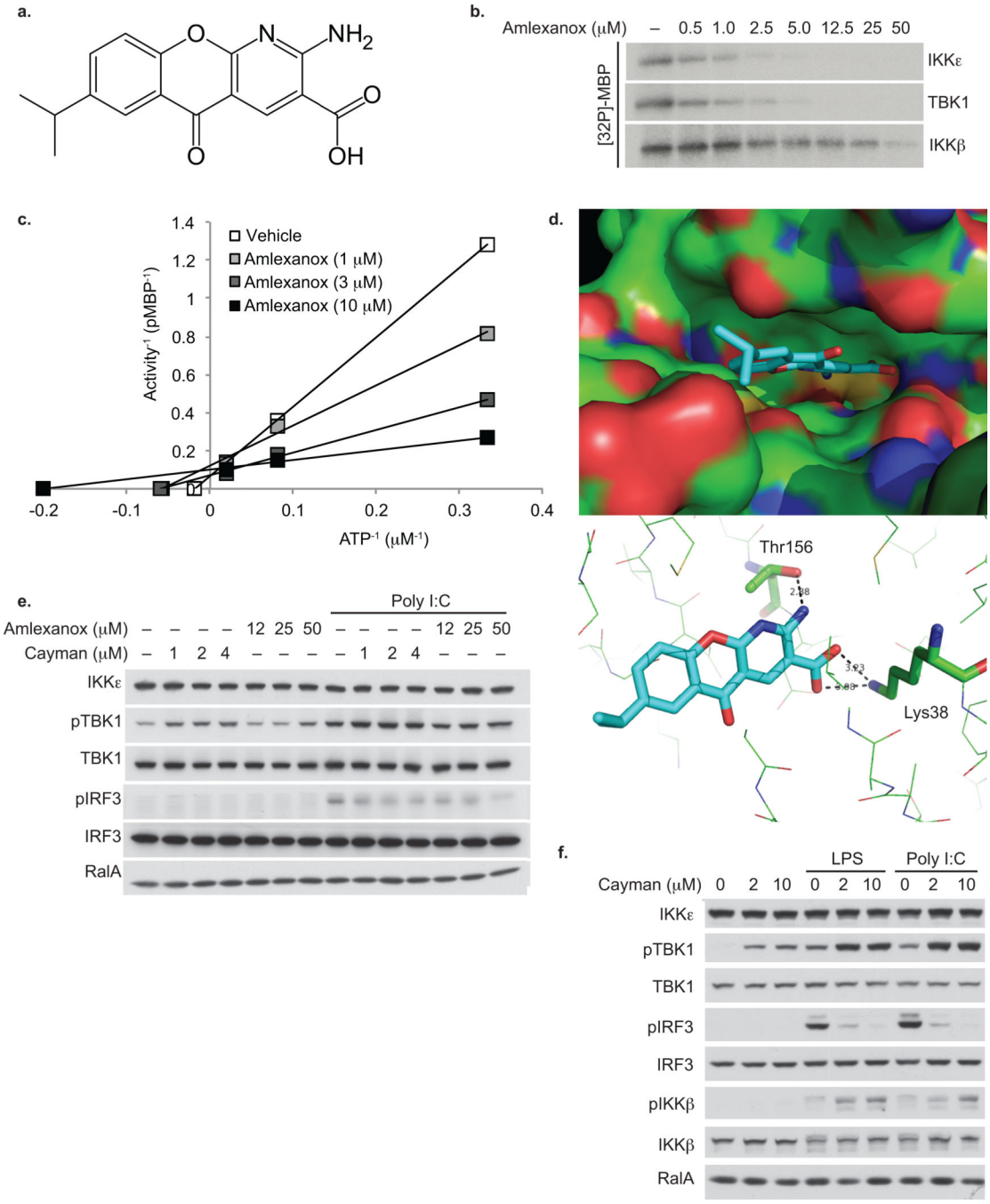

Figure 2. Amlexanox is a specific inhibitor of IKKε and TBK1

(**a**) Stick diagram of amlexanox structure. (**b**) Dose response of amlexanox inhibition of IKKε and TBK1 activity as determined by MBP phosphorylation showing an IC_{50} of approximately 1–2 μM. Results were replicated in more than three experiments. (**c**) Lineweaver-Burke plot demonstrating competition of amlexanox with ATP for inhibition of IKKε. Results are representative of multiple experiments. (**d**) Model of amlexanox binding to the ATP binding site of TBK1; top panel: Surface model showing the binding of amlexanox in the active site of TBK1; bottom panel: Hydrogen bonding of amlexanox

(cyan) in the active site of TBK1. (**e**) TBK1 phosphorylation at Ser172 and IRF3 phosphorylation at ser396 in 3T3-L1 adipocytes treated with amlexanox or cayman with and without poly I:C. Results were replicated in multiple experiments. RalA is a loading control. (**f**) IRF3, IKKβ and TBK1 phosphorylation in RAW264.7 cells treated with cayman, LPS and poly I:C. Results were replicated in multiple experiments. RalA is a loading control.

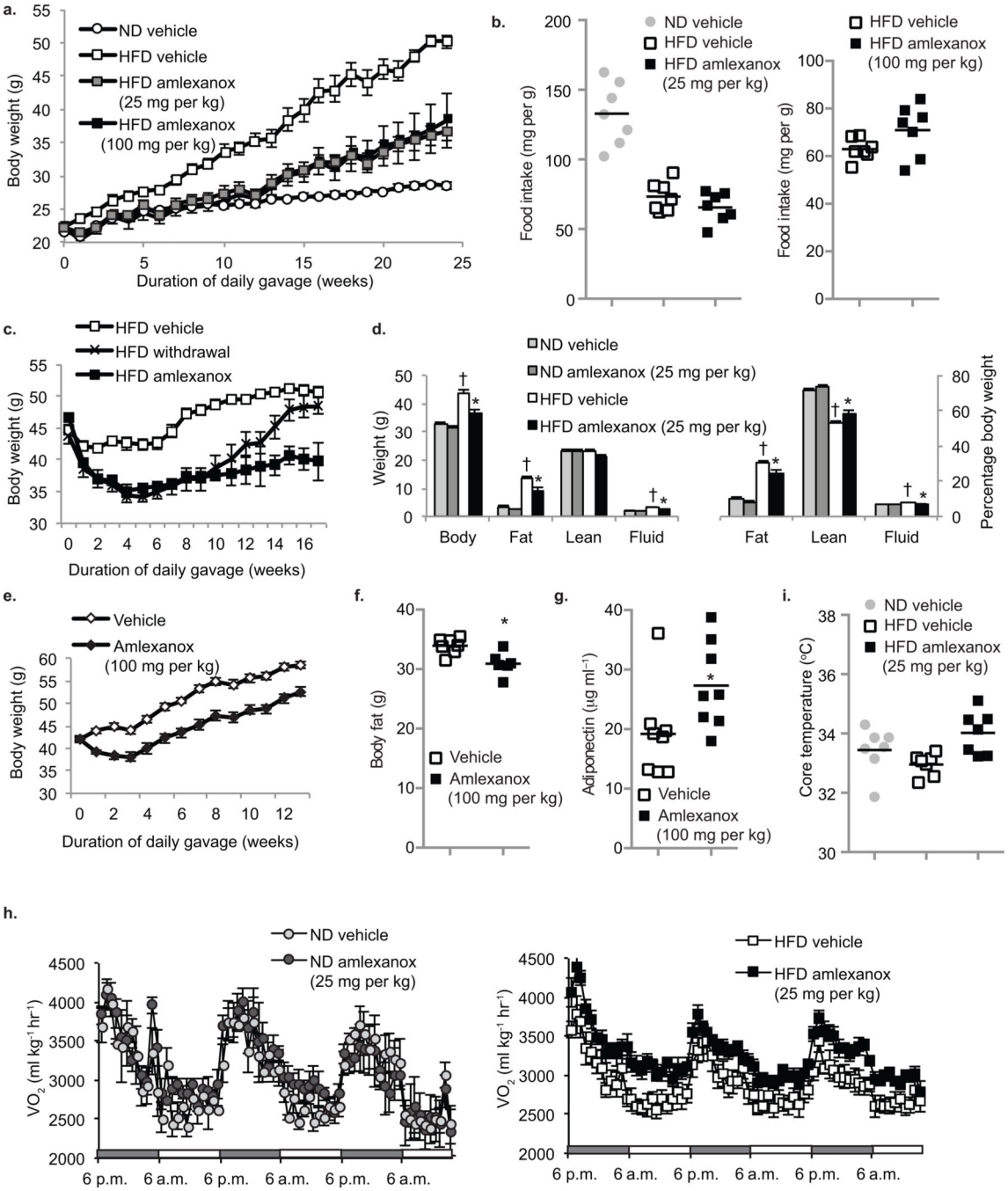

Figure 3. Daily amlexanox gavage both prevents and reverses diet-induced or genetic obesity

(**a**) Body weight of mice treated preventatively with amlexanox 25 mg per kg (grey squares) 100 mg per kg (black squares) or vehicle control (white squares = HFD, white circles = ND) (*n*=5 per group). (**b**) Food intake after one week treatment (left panel) or six weeks preventative gavage (right panel) ND vehicle (grey circles) HFD amlexanox (black squares) or HFD vehicle (white squares). (*n* = 5–7 per group) (**c**) Body weight of treatment group: amlexanox (black squares) or vehicle control (white squares). Mice maintained on ND and gavaged with vehicle control are also shown (white circles). (*n*=7 per group). (**d**) Body

weight of mice treated preventatively with amlexanox (black squares) or vehicle control (white squares), treatment withdrawn after eight weeks (black Xs) (*n*=7 per group). (**e**) Total (left panel) and relative (right panel) fat and lean body mass of mice in treatment group. ND vehicle control: light grey bars, ND amlexanox: dark grey bars, HFD vehicle control: white bars and HFD amlexanox: black bars. (*n*=4 for ND groups, *n*=8 for HFD groups). (**f**) Body weight of ob/ob mice gavaged with amlexanox (black diamonds) or vehicle control (white diamonds) (*n*=8 per group). (**g**) Total body fat mass of ob/ob mice gavaged with amlexanox (black bars) or vehicle control (white bars) (*n*=6 per goup). (**h**) Serum adiponectin levels in ob/ob mice gavaged with amlexanox (black bars) or vehicle control (white bars). (*n*=8 per group). (**i**) Oxygen consumption (VO_2) of mice in treatment group; ND (left panel – light grey circles = vehicle, dark grey circles = amlexanox) and HFD (right panel – white squares = vehicle, black squares = amlexanox). (*n*=4 for ND groups, *n*=8 for HFD groups). HFD amlexanox treated mean values are significantly higher than HFD vehicle mean values during all three light and dark cycles, *P* value < 0.05. (**j**) Core body temperature in ND mice gavaged with vehicle (grey bar), HFD mice gavaged with vehicle (white bar) or amlexanox (black bar). * *P* value < 0.05 HFD vehicle control versus HFD amlexanox treated or ob/ob vehicle control versus ob/ob amlexanox treated. † *P* value < 0.05 ND vehicle control versus HFD vehicle control.

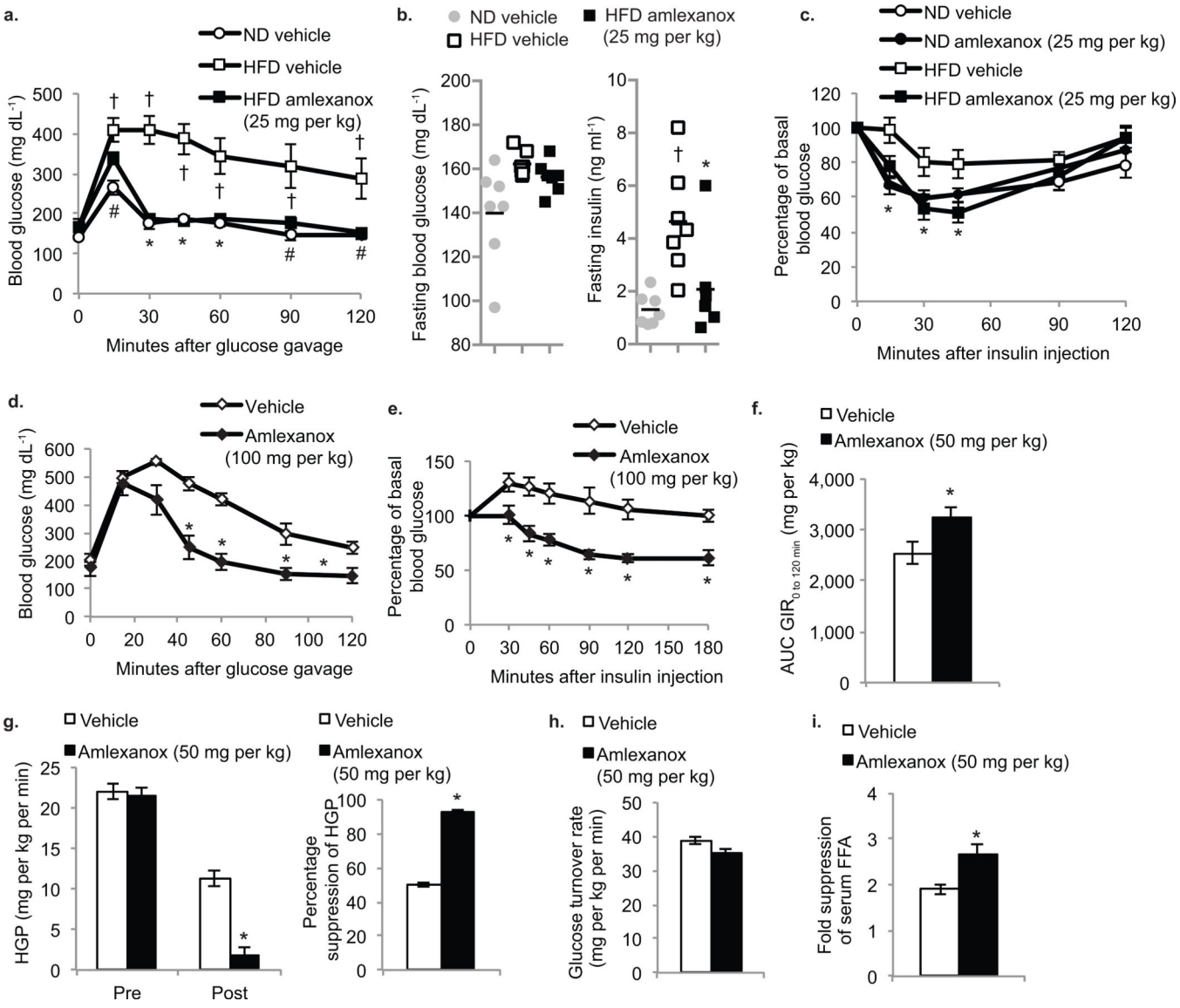

Figure 4. Amlexanox treatment improves insulin sensitivity and glucose tolerance

(**a**) Oral glucose tolerance test in preventative group. Vehicle control (ND-white circles, HFD-white squares), HFD amlexanox (black squares). (*n*=5 per group). (**b**) Fasting blood glucose and serum insulin levels in treatment group: ND vehicle control (grey bars), HFD vehicle control (white bars) and HFD amlexanox treated (black bars). (*n*=8 per group). (**c**) Insulin tolerance test of treatment group. ND vehicle control (white circles), ND amlexanox (black circles), HFD vehicle control (white squares) HFD amlexanox (black squares). (*n*=8 per group). (**d**) Oral glucose tolerance test of ob/ob mice gavaged with amlexanox (black diamonds) or vehicle control (white diamonds) (*n*=8 per group). (**e**) Insulin tolerance test in ob/ob mice gavaged with amlexanox (black diamonds) or vehicle control (white diamonds). (*n*=8 per group). (**f–i**) Hyperinsulinemic euglycemic clamp in amlexanox (50 mg per kg-black bars) and vehicle (white bars) treated HFD mice (*n*=9 per group) (**f**) Area under the curve for glucose infusion rate during clamp. (**g**) Hepatic glucose production before and after the clamp (left panel) and percent suppression of hepatic glucose production (right

panel). (**h**) Glucose turnover rate during the clamp. (**i**) Fold suppression of serum free fatty acid (FFA) levels during the clamp. * *P* value < 0.05 HFD vehicle control versus HFD amlexanox treated, or ob/ob vehicle control versus ob/ob amlexanox treated. † *P* value <0.05 ND vehicle control versus HFD vehicle control

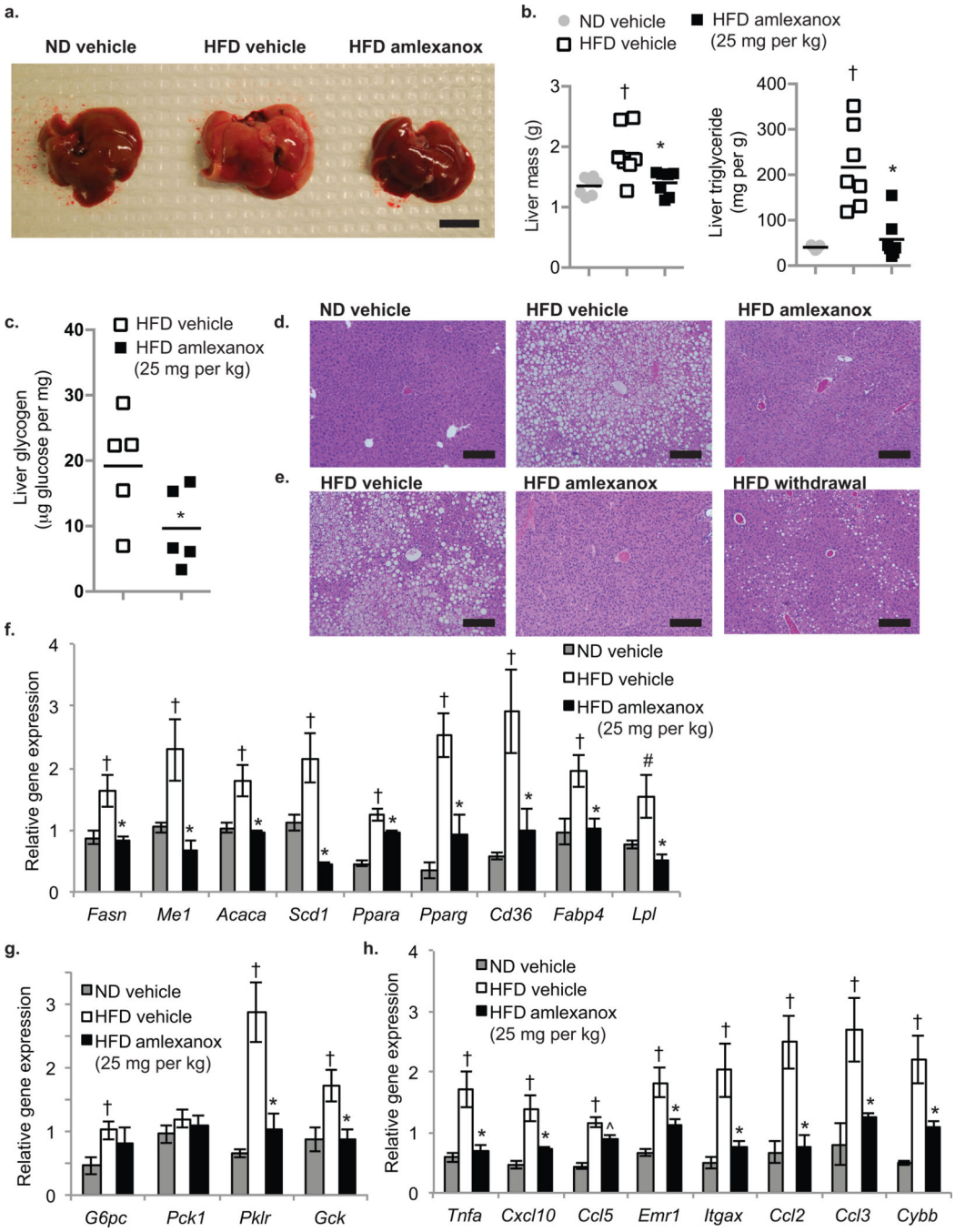

Figure 5. Amlexanox treatment reverses hepatic steatosis

(**a**) Macroscopic pictures of the liver; left: ND vehicle control, middle: HFD vehicle control; right: HFD gavaged daily with amlexanox (scale bar = 1 cm). (**b**) Total liver weight (left panel) and triglyceride content (right panel) of mice on ND (grey bars) or HFD gavaged with vehicle (white bars) or amlexanox (black bars). (*n*=6 per group). (**c**) Liver glycogen content in HFD mice treated with amlexanox (black bars) or vehicle (white bars). (*n*=5 per group). (**d,e**) Representative images of hematoxylin and eosin (H and E)-stained liver (scale bars = 2 mm). (**d**) left: ND vehicle control, middle: HFD vehicle control; right: HFD treated

with amlexanox. (**e**) left: HFD vehicle control, middle: HFD treated with amlexanox; right: HFD amlexanox withdrawal for ten weeks after eight weeks treatment. Expression of (**f**) lipid metabolism genes, (**g**) glucose metabolism genes, and (**h**) inflammatory genes and macrophage markers in livers of mice in treatment group. (**f–h**) Grey bars: ND vehicle control, white bars: HFD vehicle control; black bars: HFD gavaged daily with amlexanox (n=6 per group). All amlexanox treatment are daily gavage. * P value < 0.05 HFD vehicle control versus HFD amlexanox treated; † P value < 0.05 ND vehicle control versus HFD vehicle control; # P value < 0.1 ND vehicle control versus HFD vehicle control.

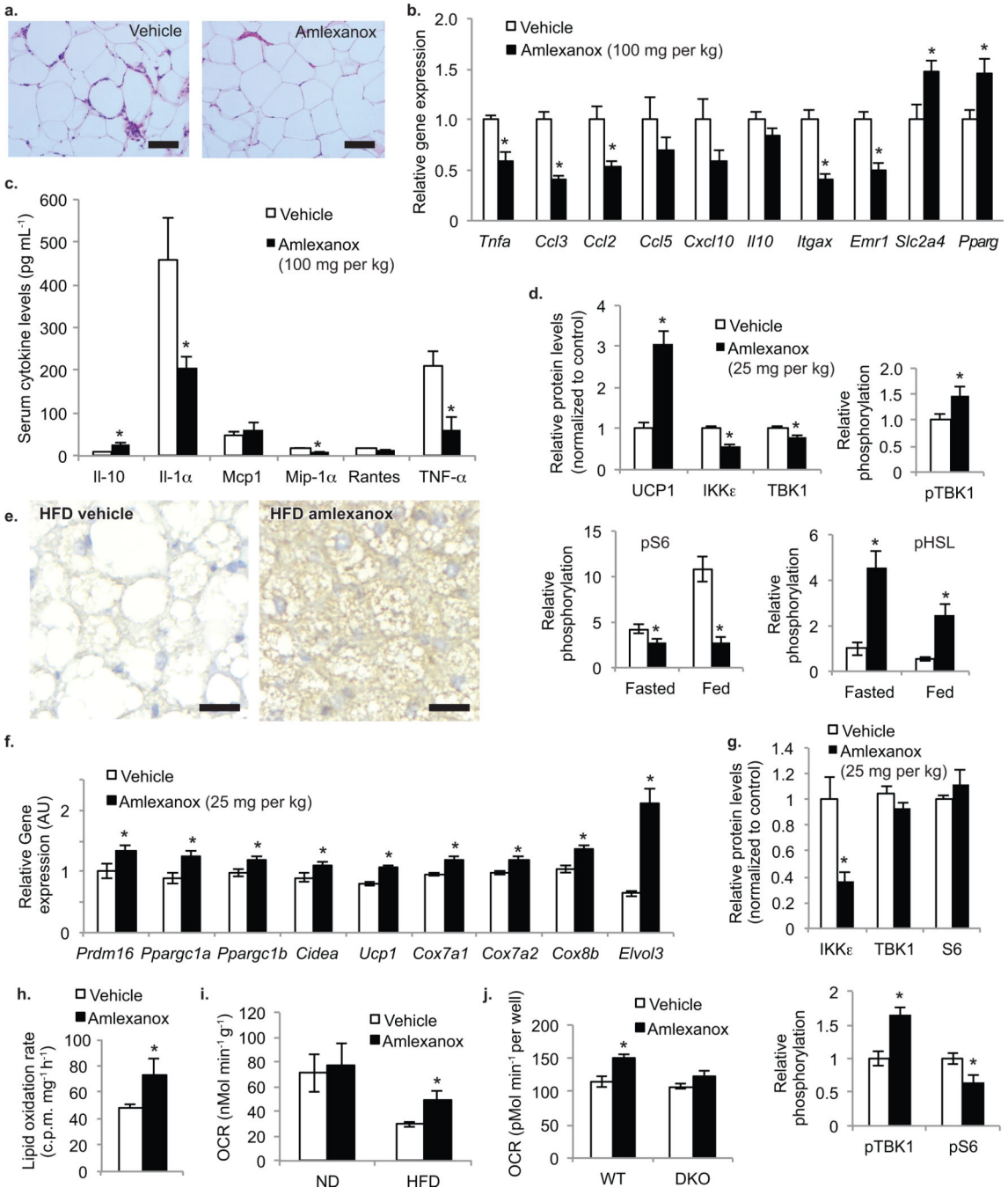

Figure 6. Amlexanox reduces inflammation and increases energy expenditure in adipose tissue

(**a**) Representative images of H and E-stained sections from WAT of ob/ob mice treated with vehicle control (left panel) or amlexanox (right panel) (scale bars = 1 mm) (**b**) Expression of inflammatory genes and macrophage markers in WAT from ob/ob mice gavaged with vehicle control (white bars) or amlexanox (black bars) (*n*=6 per group). (**c**) Serum cytokine levels in ob/ob mice gavaged with vehicle control (white bars) or amlexanox (black bars). (*n*=6 per group). (**d**) Quantified protein and phosphorylation levels in WAT from mice treated with amlexanox (back bars) or vehicle control (white bars)

western blot–Supplementary Fig. 5b, online. (**e**) BAT stained for UCP1 protein levels in HFD vehicle control (left) and amlexanox treated mice (right) (scale bars = 200 μm). (**f**) Expression of BAT specific markers in BAT; white bars: HFD vehicle control; black bars: HFD treated with amlexanox (*n*=8 per group). (**g**) Quantified protein and phosphorylation levels in BAT from mice treated with amlexanox (black bars) or vehicle control (white bars) western blot–Supplementary Fig. 5h, online. (**h**) Lipid oxidation rate in *ex vivo* BAT treated with amlexanox (black bar) or vehicle control (white bar). (*n*=6 per group). (**i**) Oxygen consumption rate in *ex vivo* BAT from ND and HFD mice treated with amlexanox (black bars) or vehicle control (white bars) (*n*=5 per group). (**j**) Oxygen consumption rate in WT and *Ikbke*/*Tbk1 double* KO (DKO) MEFs treated with amlexanox (black bars) or vehicle control (white bars). (*n*=5 wells per group). * *P* value < 0.05 vehicle control versus amlexanox treated.